Passively Q-switched self-frequency doubling Nd^{3+}:$ReCa_4O(BO_3)_3$ (Re = Y, Gd) lasers with tin diselenide as a saturable absorber

Yuxiang Sun (孙玉祥)[1], Mengxia Wang (王梦霞)[1], Xinle Wang (王新乐)[1], Ying Zhou (周 莹)[1], Bo Wang (王 波)[1,2], Zhengping Wang (王正平)[1,2,*], Fapeng Yu (于法鹏)[1,], and Xinguang Xu (许心光)[1,2]**

[1]*State Key Laboratory of Crystal Materials, Shandong University, Jinan 250100, China*
[2]*Key Laboratory of Functional Crystal Materials and Device (Shandong University), Ministry of Education, Jinan 250100, China*
**Corresponding author: zpwang@sdu.edu.cn; **corresponding author: fapengyu@sdu.edu.cn*
Received January 19, 2019; accepted March 14, 2019; posted online May 21, 2019

With tin diselenide ($SnSe_2$) film as a saturable absorber (SA), the passively Q-switched self-frequency doubling (SFD) lasers were realized in Nd^{3+}:$ReCa_4O(BO_3)_3$ (Re = Y, Gd) crystals. For Nd:$YCa_4O(BO_3)_3$ crystal, the maximum average output power at 532 nm was 19.6 mW, and the corresponding pulse repetition frequency, pulse duration, single pulse energy, and peak power were 17.6 kHz, 91.9 ns, 1.1 μJ, and 12.1 W, respectively. For Nd:$GdCa_4O(BO_3)_3$ crystal, these values were 14.5 mW, 22.1 kHz, 48.7 ns, 0.66 μJ, and 13.5 W.
OCIS codes: 140.3580, 140.3540, 160.4236, 160.4330.
doi: 10.3788/COL201917.061402.

Recently, two-dimensional (2D) transition metal dichalcogenides (TMDCs) or transition metal diselenides (TMDSs) have attracted great attention for potential applications in the field of nonlinear optics[1–6] due to their special physical properties, like sizable bandgap, layer-dependent characteristic, and broadband saturable absorption[7–12]. Molybdenum disulfide (MoS_2) is a representative TMDC. Monolayer MoS_2 is a direct bandgap semiconductor, whereas the gap of multilayer MoS_2 is indirect[13,14]. In such a material, the atoms within the same layer are held together by a strong covalent bond, while the interlayer force is a weak van der Waals interaction. Therefore, few-layer MoS_2 nanosheets can be exfoliated easily. Its unique and significant advantages can be applied to many fields.

Among the nonlinear optical applications, saturable absorption is an important one that can develop into optical modulators for passive Q-switching or mode-locking to obtain large energy and high peak power laser pulses. Using MoS_2 as a saturable absorber (SA), the passively Q-switched (PQS) lasers were reported at 1.06, 1.08, 1.42, and 2.1 μm[15–17]. Stable Q-switched operation was also achieved for the tunable laser from 1030 to 1070 nm[18]. Besides, $MoSe_2$ film was reported as the SA of Yb-, Er-, and Tm-doped fiber lasers[19,20]. Recently, $GaSe/SnS_2$ composite nanomaterial and CdTe/CdS quantum dots also realized PQS operations[21,22]. As for passive mode-locking, many TMDCs and TMDSs nanomaterials, including $MoTe_2/WTe_2$[23], SnS_2[24], MoS_2[25], WS_2[26,27], and ReS_2[28], have been used in Er-doped or Yb-doped fiber lasers.

Tin diselenide ($SnSe_2$) is a newly developed IV–VI group TMDS and possesses many excellent photoelectronic properties, such as controllable band gap, fast response, high electronic affinity, and large modulation depth[29–33]. Its saturable absorption property has been used in the passive Q-switching of waveguide, fiber, and crystal lasers at 1 μm waveband[34–36]. In this Letter, we reported its PQS performances in Nd:$ReCa_4O(BO_3)_3$ (Nd:ReCOB) (Re = Y, Gd) self-frequency doubling (SFD) lasers. The optimum pulse width, pulse energy, and peak power reached 48.7 ns, 1.1 μJ, and 13.5 W, respectively. As we have known, it is the first time, to the best of our knowledge, that a 2D nanomaterial is used to generate SFD laser pulses. Because SFD is a convenient, cheap route to obtain a visible (VIS) laser, its successful cooperation with 2D nanomaterials will be helpful for larger scale production and lower cost, as well as superior properties. Such green pulsed lasers will hopefully obtain important applications in many scopes, such as three-dimensional laser scanning, data storage, contamination detection, spectroscopy, and microsurgery.

The schematic of the experimental setup is shown in Fig. 1. An 808 nm fiber-coupled laser diode (LD) (Limo35-F100-DL808-LM) with a core diameter of 100 μm and numerical aperture (NA) of 0.22 served as the pump source. An optical coupling system (OCS) was used to collimate and focus the pump beam into the laser crystal with a beam transfer ratio of 1:1. The SFD laser crystal was 10 mm thick Nd:$YCa_4O(BO_3)_3$ (Nd:YCOB) or Nd:$GdCa_4O(BO_3)_3$ (Nd:GdCOB), which was processed along the type-I phase-matching direction for 1064 nm fundamental light. Its input face was high transmission (HT) coated at 808 nm and high reflection (HR) coated at 1064 and 532 nm, which served as the total reflection mirror of the laser resonator. Its output face was

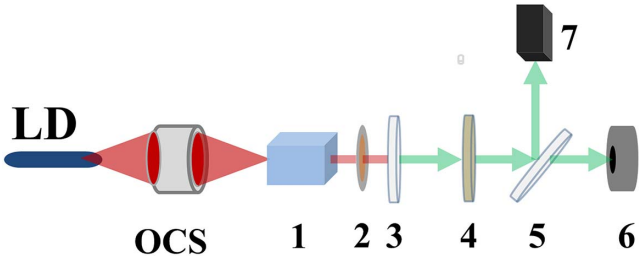

Fig. 1. Experimental set-up of $SnSe_2$ PQS SFD laser. 1, SFD crystal; 2, $SnSe_2$ SA; 3, output mirror; 4, filter; 5, beam splitter; 6, power meter; 7, oscilloscope.

antireflection (AR) coated at 1064 and 532 nm and HR coated at 808 nm. The crystal was wrapped with indium foil and then mounted into a water-cooled copper block, whose temperature was kept at 15°C. The output mirror was planar, which was HR coated at 1064 nm and HT coated at 532 nm. The total cavity length was about 16 mm. To accurately measure the output power of the SFD green laser, a filter was used to eliminate the leaked fundamental wave and pump light. The temporal behaviors of the laser pulses were monitored by a 1 GHz digital oscilloscope (DPO 7104, Tektronix Inc.) with a suitable photodiode detector (Model 1621, New Focus, response time 1 ns, decay time 1.5 ns).

Based on the liquid-phase exfoliation (LPE) method, $SnSe_2$ dispersion solution was prepared. Firstly, 0.1 g $SnSe_2$ powder was added into 10 mL alcohol (30%). Then, the mixture was placed in an ultrasonic cleaner for 12 h. Subsequently, it was centrifuged at a rate of 3000 r/min for 15 min. The top two-thirds of the dispersion was collected by a pipette. Because of the removal of large sedimentations, the stability as well as the transmittance of the extracted dispersion improved significantly. Next, the $SnSe_2$ dispersion was mixed with a 4 wt. % polyvinyl alcohol (PVA) solution at the volume ratio of 1:2. Afterward, the $SnSe_2$-PVA solution was placed in the ultrasonic cleaner for 2 h. Finally, the $SnSe_2$-PVA dispersion solution was dropped on a 1 mm thick quartz substrate, and the dried component was used as the SA for solid-state laser experiments. The samples at different stages are shown in Fig. 2.

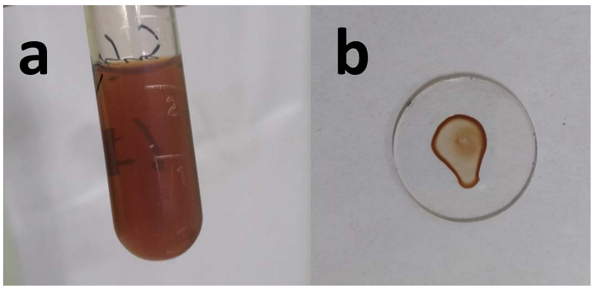

Fig. 2. a, The $SnSe_2$-PVA dispersion solution. b, The SA with $SnSe_2$-PVA thin film.

The linear transmission spectrum of the $SnSe_2$ SA was measured in the range of 200–1600 nm with a UV/VIS/near-IR (NIR) spectrophotometer (Hitachi UH4150). The result is shown in Fig. 3. As a comparison, a curve of blank quartz substrate was also measured and demonstrated. As can be seen from Fig. 3, a broad, nearly constant transmission of 77% was measured from 700 to 1600 nm. The net absorbance of the $SnSe_2$-PVA film was about 90% at the 1000 nm waveband. This absorbance was similar with the value reported by Cheng *et al.*[34]. So, in terms of thickness, our $SnSe_2$-PVA film was basically equivalent to their sample, i.e., the chemical vapor deposition (CVD) prepared pure $SnSe_2$ film with a thickness of 22 nm.

Using an optical parametric oscillator (OPO) laser (Continuum, Horizon) with a wavelength of 1064 nm, pulse width of 6 ns, and repetition rate of 10 Hz, we directly investigated the nonlinear saturable absorption property of the $SnSe_2$-PVA film. As a background experiment, the transmission of the blank quartz substrate was also measured under the same conditions, and no nonlinear absorption behavior was observed. The saturable absorption experimental data are displayed in Fig. 4, which could be fitted by the following formula[37]:

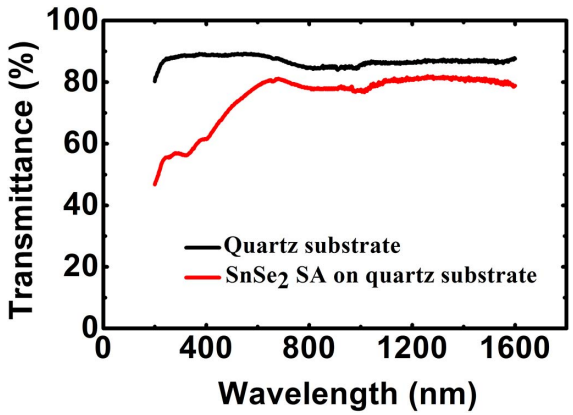

Fig. 3. Transmission spectra of $SnSe_2$ SA and blank quartz substrate.

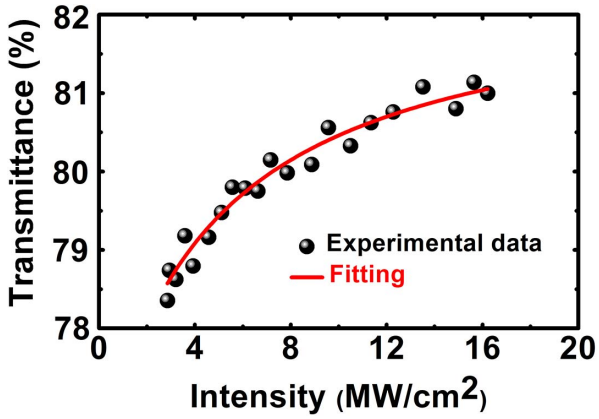

Fig. 4. Transmittance variation of $SnSe_2$ SA with incident power intensity of 1064 nm.

$$T = A\exp\left(\frac{-\delta T}{1+\frac{I}{I_s}}\right),$$

where T, A, δT, I, and I_s are the transmittance of the sample, normalized constant, absolute modulation depth, incident light intensity, and saturation intensity, respectively. The absolute modulation depth of the $SnSe_2$ SA was fitted to be 7.9%, and the fitted saturation intensity I_s was 4.5 MW/cm^2. When the incident intensity was 16 MW/cm^2, the actual modulation depth of this component was 2.3% (78.7% → 81.0%).

When the $SnSe_2$ SA was removed from the resonator, the continuous-wave (cw) SFD laser performance was measured. By inserting the $SnSe_2$ SA into the laser cavity, the PQS operation was realized. The detailed results of the Nd:YCOB crystal are shown in Fig. 5, and those of the Nd:GdCOB crystal are shown in Fig. 6.

As presented in Fig. 5a, the maximum cw green power of the Nd:YCOB crystal was 315 mW at an incident pump power of 5.01 W. The corresponding threshold pump power was 0.33 W. For PQS operation, the threshold pump power was 2.1 W. Here, we stated that in our experiments the SFD threshold was always identical to the fundamental laser threshold, whether for cw SFD operation or for Q-switched SFD operation. Compared with the cw laser, the PQS laser exhibited much higher pump threshold and much smaller output power. This performance could be attributed to the large inserting loss brought by the $SnSe_2$ SA, whose quartz substrate was not AR coated at 1064 or 532 nm. This situation meant that large unsaturable loss was added to the laser cavity, which could be improved in the future. After the insertion of $SnSe_2$, we did not observe cw operation at any input power level. Stable Q-switching operation was acquired in the pump region of 2.4–4.1 W. The highest Q-switched SFD output power was 19.6 mW at the incident pump power of 4.13 W. The pulse characteristics are demonstrated in Figs. 5b and 5c. With the increase of pump power, the pulse repetition rate, single pulse energy, and peak power all elevated, and the pulse width decreased. The shortest pulse width was 91.9 ns, and the highest pulse repetition rate was 17.6 kHz, as shown in Fig. 5d. In the pulse train, the timing jitter of the pulse amplitude was ±12%. The single pulse energy and peak power corresponding to the Fig. 5d were 1.1 μJ and 12.1 W, respectively. Further enhancing the pump power, the pulse performance degraded apparently, and the pulse sequence became disordered, although no obvious damage was observed on the $SnSe_2$ SA.

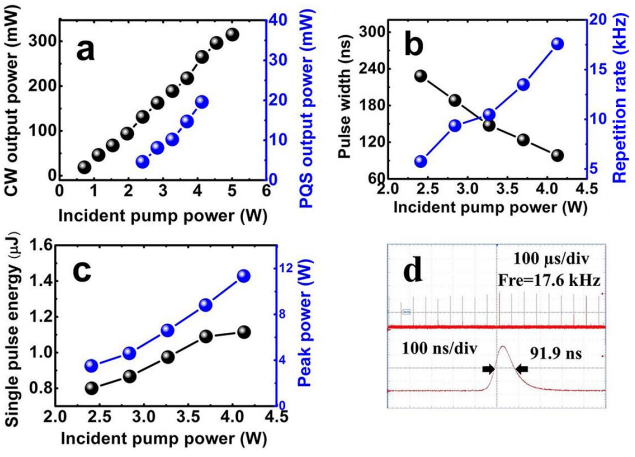

Fig. 5. PQS SFD laser characteristics of Nd:YCOB crystal with $SnSe_2$ as SA. a, Output powers of cw and PQS lasers. b, Pulse width and repetition rate. c, Single pulse energy and peak power. d, Pulse train with a repetition rate of 17.6 kHz and single pulse waveform with a width of 91.9 ns.

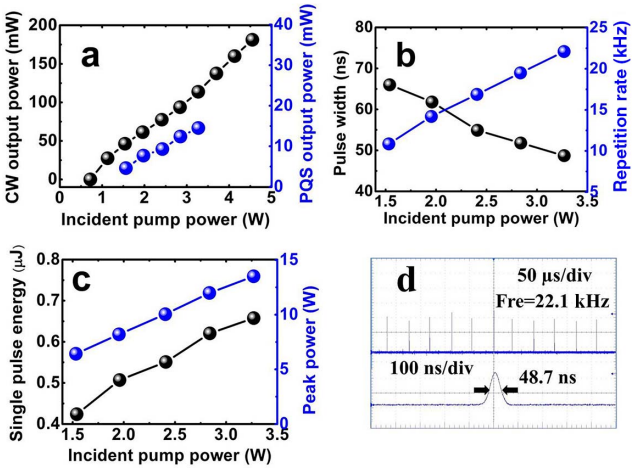

Fig. 6. PQS SFD laser characteristics of Nd:GdCOB crystal with $SnSe_2$ as SA. a, Output powers of cw and PQS lasers. b, Pulse width and repetition rate. c, Single pulse energy and peak power. d, Pulse train with a repetition rate of 22.1 kHz and single pulse waveform with a width of 48.7 ns.

For the Nd:GdCOB crystal, the maximum cw green power was 181 mW, which was obtained at an incident pump power of 4.55 W. Compared with the cw SFD laser operation, the Q-switched threshold pump power increased to 1.15 W from 0.72 W. The pump power region for stable Q-switching was 1.5–3.3 W. When the pump power was higher than 3.3 W, the pulse sequence turned disordered, but no damage was observed on the SA, just like the phenomenon of Nd:YCOB when the pump power exceeded 4.1 W. At an incident pump power of 3.3 W, the maximum Q-switched average output power was 14.5 mW. The detailed pulse characteristics versus the incident pump powers are shown in Figs. 6a–6c. The maximum single pulse energy and the highest peak power were 0.66 μJ and 13.5 W, respectively, corresponding to the shortest pulse width of 48.7 ns and the highest repetition rate of 22.1 kHz, as demonstrated in Fig. 6d. In the pulse train, the timing jitter of the pulse amplitude was ±14%.

Lastly, it should be noted that under our experimental conditions the PQS SFD operations were stable; for pulsed Nd:YCOB and Nd:GdCOB SFD lasers, their fluctuations at the largest output powers were both smaller than ±1 mW in 20 min.

In this Letter, $SnSe_2$-PVA film was successfully prepared and employed as the SA of a Nd:ReCOB (Re = Y, Gd) SFD green laser to realize PQS operation. The best PQS results included 19.6 mW of average output power, 48.7 ns of pulse width, 1.1 μJ of single pulse energy, and 13.5 W of peak power. Compared with the cw output power of 200–300 mW in similar conditions, the peak power for PQS operation elevated by more than 40 times. It will be favorable for some special applications, such as nonlinear optics, microsurgery, contamination detection and ion spectroscopy. In short, the present research raises a novel, convenient, and low-cost way to fabricate a pulsed VIS laser. It associates the new developed 2D material SA technology with the relatively traditional SFD laser technology and has potential for large scale production and wide application.

This work was supported by the Natural Science Foundation of Shandong Province (No. ZR2017MF031).

References

1. Y. Li, Y. Rao, K. F. Mak, Y. You, S. Wang, C. R. Dean, and T. F. Heinz, Nano Lett. **13**, 3329 (2013).
2. K. Wang, J. Wang, J. Fan, M. Lotya, A. O'Neill, D. Fox, Y. Feng, X. Zhang, B. Jiang, Q. Zhao, H. Zhang, J. N. Coleman, L. Zhang, and W. J. Blau, ACS Nano **7**, 9260 (2013).
3. R. Wang, H. C. Chien, J. Kumar, J. Kumar, H. Y. Chiu, and H. Zhao, ACS Appl. Mater. Int. **6**, 314 (2013).
4. J. J. Wu, Y. R. Tao, X. C. Wu, and Y. Chun, J. Alloy. Compd. **713**, 38 (2017).
5. S. Zhang, N. Dong, N. McEvoy, M. O'Brien, S. Winters, N. C. Berner, C. Yim, Y. Li, X. Zhang, Z. Chen, L. Zhang, G. S. Duesberg, and J. Wang, ACS Nano **9**, 7142 (2015).
6. H. Zeng, G. B. Liu, J. Dai, Y. Yan, B. Zhu, R. He, L. Xie, X. Xu, X. Chen, W. Yao, and X. Cui, Sci. Rep. **3**, 1608 (2013).
7. J. A. Wilson and A. D. Yoffe, Adv. Phys. **18**, 193 (1969).
8. A. D. Yoffe, Adv. Phys. **42**, 173 (1993).
9. Q. Wang, K. Kalantar-Zadeh, A. Kis, J. N. Coleman, and M. S. Strano, Nat. Nanotechnol. **7**, 699 (2012).
10. K. Zhou and H. Zhang, Small **11**, 3206 (2015).
11. M. L. Liu, Y. Y. Ouyang, H. R. Hou, W. J. Liu, and Z. Y. Wei, Chin. Opt. Lett. **17**, 020006 (2019).
12. B. Guo, Chin. Opt. Lett. **16**, 020004 (2018).
13. A. Splendiani, L. Sun, Y. Zhang, T. Li, J. Kim, C. Chim, G. Galli, and F. Wang, Nano Lett. **10**, 1271 (2010).
14. K. F. Mak, C. Lee, J. Hone, J. Shan, and T. F. Heinz, Phys. Rev. Lett. **105**, 136805 (2010).
15. S. Wang, H. Yu, H. Zhang, A. Wang, M. Zhao, Y. Chen, L. Mei, and J. Wang, Adv. Mater. **26**, 3538 (2014).
16. B. Xu, Y. Cheng, Y. Wang, Y. Huang, J. Peng, Z. Luo, H. Xu, Z. Cai, J. Weng, and R. Moncorge, Opt. Express **22**, 28934 (2014).
17. Y. Xue, Z. D. Xie, Z. L. Ye, X. P. Hu, J. L. Xu, and H. Zhang, Chin. Opt. Lett. **16**, 020018 (2018).
18. R. I. Woodward, E. J. R. Kelleher, R. C. T. Howe, G. Hu, F. Torrisi, T. Hasan, S. V. Popov, and J. R. Taylor, Opt. Express **22**, 31113 (2014).
19. H. Ahmad, F. A. A. Rashid, S. R. Azzuhri, M. A. M. Salim, R. A. Shaharuddin, M. A. Ismail, and M. Z. A. Razak, Laser Phys. Lett. **13**, 115102 (2016).
20. R. I. Woodward, R. C. T. Howe, T. H. Runcorn, G. Hu, F. Torrisi, E. J. R. Kelleher, and T. Hasan, Opt. Express **23**, 20051 (2015).
21. Q. Song, B. Zhang, and G. Wang, Infrared Phys. Technol. **93**, 87 (2018).
22. B. Xu, S. Luo, X. Yan, J. Li, J. Lan, Z. Luo, H. Xu, Z. Cai, H. Dong, J. Wang, and L. Zhang, IEEE J. Sel. Top. Quant. **23**, 1900507 (2017).
23. D. Mao, B. Du, D. Yang, S. Zhang, Y. Wang, W. Zhang, X. She, H. Cheng, H. Zeng, and J. Zhao, Small **12**, 1489 (2016).
24. K. Niu, R. Sun, Q. Chen, B. Man, and H. Zhang, Photon. Res. **6**, 72 (2018).
25. H. Zhang, S. B. Lu, J. Zheng, J. Du, S. C. Wen, D. Y. Tang, and K. P. Loh, Opt. Express **22**, 7249 (2014).
26. D. Mao, S. Zhang, Y. Wang, X. Gan, W. Zhang, T. Mei, Y. Wang, Y. Wang, H. Zeng, and J. Zhao, Opt. Express **23**, 27509 (2015).
27. K. Wu, X. Zhang, J. Wang, X. Li, and J. Chen, Opt. Express **23**, 11453 (2015).
28. D. Mao, X. Cui, X. Gan, M. Li, W. Zhang, H. Lu, and J. Zhao, IEEE J. Sel. Top. Quant. **24**, 1100406 (2018).
29. J. M. Gonzalez and I. I. Oleynik, Phys. Rev. B **94**, 125443 (2016).
30. P. Yu, X. Yu, W. Lu, H. Lin, L. Sun, K. Du, F. Liu, W. Fu, Q. Zeng, Z. Shen, C. Jin, Q. Wang, and Z. Liu, Adv. Funct. Mater. **26**, 137 (2016).
31. R. Y. Wang, M. A. Caldwell, R. G. D. Jeyasingh, S. Aloni, R. M. Shelby, H. S. P. Wong, and D. J. Milliron, J. Appl. Phys. **109**, 113506 (2011).
32. Y. Su, M. A. Ebrish, E. J. Olson, and S. J. Koester, Appl. Phys. Lett. **103**, 263104 (2013).
33. E. P. Mukhokosi, S. B. Krupanidhi, and K. K. Nanda, Sci. Rep. **7**, 15215 (2017).
34. C. Cheng, Z. Li, N. Dong, J. Wang, and F. Chen, Opt. Express **25**, 6132 (2017).
35. R. Sun, H. Zhang, and N. Xu, Laser Phys. **28**, 085105 (2018).
36. Q. Song, B. Y. Zhang, and G. J. Wang, Optik **174**, 35 (2018).
37. M. Wang, F. Zhang, Z. Wang, Z. Wu, and X. Xu, Opt. Express **26**, 4085 (2018).